Crystal structure of bacterial CYP116B5 heme domain: New insights on class VII P450s structural flexibility and peroxygenase activity

(Article begins on next page)

11 February 2025

Crystal structure of bacterial CYP116B5 heme domain: new insights on class VII P450s structural flexibility and peroxygenase activity.

Alberto Ciaramella[a], Gianluca Catucci[a], Gianfranco Gilardi[a,b], Giovanna Di Nardo[a,b,*]

[a] Department of Life Sciences and Systems Biology, University of Torino, Via Accademia Albertina 13, Torino, Italy

[b] CrisDi, Interdepartmental Center for Crystallography, University of Torino, Via Pietro Giuria 7, Torino, Italy

*Corresponding author:

Giovanna Di Nardo

Via Accademia Albertina 13, 10123, Torino, Italy

e-mail: giovanna.dinardo@unito.it

Telephone number: +39 011 6704689

Fax number: +39 011 6704508

Abstract

Class VII cytochromes P450 are self-sufficient enzymes carrying a phthalate family oxygenase-like reductase domain and a P450 domain fused in a single polypeptide chain. The biocatalytic applications of CYP116B members are limited by the need of the NADPH cofactor and the lack of crystal structures as a starting point for protein engineering. Nevertheless, we demonstrated that the heme domain of CYP116B5 can use hydrogen peroxide as electron donor bypassing the need of NADPH.

Here, we report the crystal structure of CYP116B5 heme domain in complex with histidine at 2.6 Å of resolution. The structure reveals the typical P450 fold and a closed conformation with an active site cavity of 284 $Å^3$ in volume, accommodating a histidine molecule forming a hydrogen bond with the water molecule present as 6th heme iron ligand. MD simulations in the absence of any ligand revealed the opening of a tunnel connecting the active site to the protein surface through the movement of F-, G- and H-helices.

A structural alignment with bacterial cytochromes P450 allowed the identification of amino acids in the proximal heme site potentially involved in peroxygenase activity.

The availability of the crystal structure provides the bases for the structure-guided design of new biocatalysts.

1. Introduction

The development of new biocatalysts for organic synthesis and for the production of novel metabolites with interesting biological activities is a relevant and challenging topic [1,2].

In this context, cytochromes P450, a superfamily of heme thiolate enzymes that catalyse different reactions on substrates that range from ethylene to complex antibiotics [3-5], are optimal candidates for different biocatalytic applications [6,7]. The interest for these enzymes is due to their ability to carry out reactions difficult to achieve with standard chemical methods and their versatility that have led to the development of many mutants with improved catalytic abilities on substrates of interest [8-13]. Indeed, some members of this superfamily have already been introduced as biocatalysts at an industrial scale for the biosynthesis of drugs [14-18].

In order to carry out their reaction, most cytochromes P450 generally need a redox partner that can be a flavin-containing protein that transfers electrons from NADPH to the P450 enzyme directly or via another protein that usually contains an iron-sulfur cluster [19]. Some exceptions are represented by class VII and class VIII cytochromes P450 that are bacterial self-sufficient enzymes with a multi-domain organization [19]. Moreover, some cytochromes P450s can use hydrogen peroxide as electron donor in a short cut of the catalytic cycle known as peroxide shunt [20].

Class VII P450s include enzymes containing a phthalate family oxygenase (PFOR)-like reductase module, accepting the electrons from NADPH and transferring them to the fused P450 domain [19, 21,22]. They have been demonstrated to be able to carry out hydroxylation, demethylation and sulfoxidation reactions on different substrates that include aromatics and fatty acids [23-25]. They have shown interesting properties such as good expression levels and thermal stability [25,26]. In addition,

we recently demonstrated that the isolated heme domain of CYP116B5 from *Acinetobacter radioresistes* S13 (CYP116B5hd) can bypass the need of the expensive NADPH cofactor and the reductase module using the so-called "peroxide shunt" that allows to accept the electrons directly from hydrogen peroxide [27]. The enzyme also has a higher tolerance to hydrogen peroxide damage compared to other bacterial enzymes and broad substrate specificity. Indeed, it is able to carry out the regioselective hydroxylation of alkanes, aromatics and diclofenac and the *N*-demethylation of tamoxifen [27,28].

Here, we report the crystal structure of CYP116B5hd that provides new insights in the structural organization of class VII cytochromes P450. Until now, only one crystal structure of a class VII P450 heme domain (CYP116B46hd) has been reported [29]. The crystal structure is compared to bacterial cytochromes P450 that use the canonical P450 catalytic cycle and to the so-called P450 peroxygenases that use the peroxide shunt. MD and docking simulations are used to study the protein flexibility, the interaction with known substrates and with the 2Fe-2S cluster-containing domain that constitutes part of the physiological electron transfer domain.

2. Material and methods

2.1 Materials

All chemicals used were purchased from Sigma Aldrich and were of the highest available purity grade. Crystallisation plates, tools and buffer were purchased from Molecular Dimension.

2.2 Expression and purification

The pET116B5 plasmid, carrying the N-terminal 6xHis-Tag heme domain of CYP116B5, was used to transform *E. coli* BL21 (DE3) cells. The expression was induced by adding 100 µM IPTG and carried out for 24 hours at 22-24°C in LB medium supplemented with 0.5 mM of δ-aminolevulinic acid. For protein purification, cells were resuspended and sonicated in a 50 mM potassium phosphate pH 6.8 buffer supplemented with 100 mM KCl, 1 mg/mL lysozyme, 1% Triton X-100, 1 mM phenylmethylsulfonyl fluoride (PMSF) and 1 mM benzamidine. Cell debris was removed by ultracentrifugation at 41,000 g for 45 minutes at 4°C.

The supernatant was loaded onto a 1 ml Nickel-ion affinity column (His-trap HP, GE Healthcare) and eluted applying a linear gradient of imidazole ranging from 20 to 200 mM. The fractions containing the protein were pooled, concentrated and loaded onto a Superdex 200 size exclusion chromatography (GE Healthcare) and eluted with 50 mM potassium phosphate pH 6.8, 200 mM KCl. The fractions containing the monomeric form of the protein with a purity ratio (A_{418nm}/A_{280nm}) > 1.3 were pooled together and concentrated using Amicon ultracentrifugation filters (30 kDa cutoff) provided by Merck. The concentration of the folded protein was evaluated from the cytochrome P450-CO complex spectrum obtained upon reduction of the protein with sodium dithionite and CO bubbling, using an extinction coefficient at 450 nm of 91,000 M^{-1} cm^{-1} [30].

2.3 Protein crystallization

Red crystals were obtained by sitting drop vapour diffusion method using freshly purified protein at a concentration of 40 mg mL^{-1} in a 100 mM potassium phosphate pH 6.8 buffer. The droplets were set up with an equal volume (1 µL) of protein and reservoir. The crystals grew up after 4-5 weeks in a reservoir solution containing 100

mM amino acids (0.02 M DL-Arginine hydrochloride, 0.02 M DL-Threonine, 0.02 M DL-Histidine monohydrochloride monohydrate, 0.02 M DL-5-Hydroxylysine hydrochloride, 0.02 M *trans*-4-hydroxy-L-proline), 0.1 M Gly-Gly, 2-amino-2-methyl-1,3-propanediol (AMPD) buffer pH 8.5, 36% v/v of a precipitant mix containing 30% w/v PEG 3000, 40% v/v 1,2,4-Bbutanetriol, 2% w/v of non-detergent sulfobetaines (NDSB) 256. This condition is included in the Morpheus II™ crystallization screening (Molecular Dimensions).

The crystals were flash-frozen in liquid nitrogen for diffraction test. The best results in terms of resolution were obtained without the addition of any cryo-protectant, since already included in the reservoir solution.

2.4 Diffraction data collection and structure determination

X-ray diffraction data were collected from a single crystal at the beamline ID23-2 at the European Synchrotron Research Facility (Grenoble, France).

The diffraction images were processed using the software DIALS [31] and Aimless [32] within the CCP4 package.

The space group is $P4_12_12$ with unit cell parameters a= 109.9 Å, b= 109.9 Å, and c= 164.2 Å, $\alpha/\beta/\gamma = 90°$ and two protein molecules per asymmetric unit.

Initial analysis of crystal solvent content using the Matthews coefficient suggested that the asymmetric unit contained one protein molecule with 48.8% solvent content [33].

The structure was solved by molecular replacement using PHASER [34] from the CCP4 package [35] and the previously solved CYP116B46 heme domain crystal structure as template (PDB ID: 6GII) [29]. The model was built using Autobuild software [36] and manual building using COOT [37]. The structure was refined by

Refmac [38] and PHENIX refine [39] to final $R_{work} = 0.20$ and $R_{free} = 0.24$ and validated using Molprobity [40]. The data collection and model refinement statistics are summarized in Table 1. UCSF Chimera was used to analyse, compare and align the structures. UCSF Chimera and PyMol softwares were used to produce images. The CASTp 3.0 server was the detection and measurements of the protein cavities [41].

2.5 UV-VIS absorbance analysis of histidine binding

Absorbance measurements of histidine ligand binding were conducted on Agilent 8453 UV-Vis spectrophotometer (diode array) at 25°C (Peltier Agilent 89090 A). Each binding experiment (three replicates) required an initial sample volume of 400 μL using a 0.1 cm × 1 cm path length quartz cuvette. Protein samples consisted of 1.5–2 μM purified CYP116B5hd in 50 mM potassium phosphate buffer pH 6.8. Spectra were recorded from 250 to 800 nm between addition of 1-10 μL aliquots of the inhibitor stock solution not to exceed 2% volume. The ligand was added in solution, gently mixed and left incubated with the protein for 2 minutes before recording the spectrum. The final concentration of histidine was 0.5 mM. The difference spectra were obtained subtracting the ligand-bound to the ligand-free form spectra.

2.6 Molecular dynamics simulations and protein docking

The molecular dynamics simulation was carried out on an Omen 880-102NL i7-8700K 16GB pc using the YASARA package [42]. Before starting the simulation, CYP116B5hd structure was optimized for hydrogen bonds in the ligand free form. The optimized structure was inserted in a simulation cell that is 10 Å larger than the

8

monomeric crystal structure of CYP116B5hd. The applied force field was AMBER14, the cell was filled with water and 0.9 % NaCl to simulate physiological conditions. The temperature was set to 298 K. Initially the structure is energy mimized throughout a simulated annealing step. Molecular dynamics was followed or 100 ns with a timestep of recording snapshots every 100 ps. Van der Waals interactions cutoff was 7.86 Å and long-range electrostatic interactions were calculated using the Particle Mesh Ewald (PME) algorithm.

The Autodock version 4.0 software [43] embedded in the YASARA structure package was employed for protein-ligand interaction studies with the protocol previously described [44]. Three known substrates of CYP116B5hd, namely *p*-nitrophenol, tamoxifen and diclofenac were first optimized for their 3D structure. After ligands optimization, histidine was removed from the crystal structure of CYP116B5hd and the molecules were molecular docking was performed. A preliminary global docking experiment was carried out performing 999 runs with a 15 × 15 × 15 Å simulation cell centered on the Fe atom. The Autodock algorithm returns a series of binding modes classified by the binding energy outputs. Among these binding modes the protein-ligand complex bearing the highest binding energy, calculated by YASARA as the mechanical energy required for disassembling a whole into separate parts (where positive energies indicate stronger binding and negative energies equate to no binding), was selected and further refined by local docking. Best complexes in terms of binding energy were then subjected to 999 runs of local docking resulting in the final docked binding poses.

For the docking of CYP116B5hd structure to its redox partner, the server ClusPro was used [45]. The balanced best model was chosen for depiction and analysis using UCSF Chimera.

2.7 Trypsin digestion

Trypsin digestion was performed as previously described [46]. The time course of the digestion, performed with 120 μg of CYP116B5hd and 1 μg of trypsin, was followed for 60 min at 37°C taking 10 μL of samples at regular intervals (2, 5, 10, 15, 20, 30, 60 min) and mixing them with 10 μL of Laemmli solution (60 mM Tris pH 6.8, 2% SDS, 12% glycerol, traces of bromophenol blue). The samples were immediately incubated at 98°C for 10 min to stop the digestion. All samples were then loaded on a SDS gel for the analysis. A control reaction without trypsin was set up for 60 minutes at 37°C.

3. Results and Discussion

3.1 Overall structure

The overall structure of CYP116B5hd shows the typical P450 fold and consists of 18 α-helices and 3 β-sheets (Figure 1A). The electron density of the generally disordered N-terminal α-helix (helix $\alpha 1$) is clearly visible as in the crystal structure of CYP116B46 [29].

A structural alignment of CYP116B5hd to representative members of different classes of bacterial cytochromes P450 (Figure S1) shows the presence of longer β2-3 -B' and B'-C loops with helix B' (aa 96-104) protruding from the protein surface (Figure 1B). This is due to an insertion that is present in different CYP116B members as well as in class IV CYP119 even if it is poorly conserved in terms of primary sequence. Helix B' is missing in some bacterial P450s whereas it protrudes outside

the protein in class IV cytochromes P450 from thermophilic bacteria, such as CYP119 (Figure 1B) [47].

The superimposition to the one of CYP116B46 shows some differences in the position of the B'-, G- and H- helices (Figure 1C-1D). Another significant difference is the presence of a well-folded and continuous F-helix in CYP116B5hd that in the CYP116B46hd structure is split by a loop. However, since the structure of CYP116B46hd is in the ligand-free form whereas the structure of CYP116B5hd is in complex with histidine, such differences can be explained with different conformations adopted by the enzymes as a consequence of ligand binding.

3.2 Active site

The active site of the protein accommodates the heme cofactor coordinated by Cys374 with a Fe-S distance of 2.5 Å (Figure 2A). The cys residue involved in heme coordination is conserved among all CYP116B members. In the crystal structure of CYP116B46, an arginine residue forms a H-bond with the carbonyl group of the Cys coordinating the heme cofactor whereas in most members of the CYP116B subfamily, this amino acid is substituted by a Lys (K377 in CYP116B5) causing the loss of the H-bond. The interactions between Arg119, Arg315, Tyr369 and His372 and the heme propionates, previously reported for CYP116B46, are all conserved (Figure 2A).

In the active site of the protein, a positive electron density shows the presence of a molecule that is bound to the heme iron directly or through the water molecule present as 6th axial ligand (Figure 2B). The heme is in plane, reflecting the presence of the 6th axial ligand. Since no ligand was added during the purification and prior to crystallization, we tried to fit into the electron density the molecules present in the reservoir cocktail used for crystallization that contained also mixtures of amino acids.

Among them, histidine is known to potentially coordinate the heme iron through the imidazole moiety. The histidine residue was found to nicely fit into the electron density in a conformation where the closest nitrogen atom is too far (4.0 Å) from the heme iron to allow direct coordination (Figure 2B). Moreover, when refining this complex, a strong positive electron density was found to be present between the histidine and the heme iron. This electron density was assigned to a water molecule bridging the heme iron and histidine (Figure 2C). In order to validate this conclusion, histidine was titrated in a solution containing CYP116B5hd to monitor its effect on the protein Soret peak by UV-vis spectroscopy. The titration did not show any shift of the Soret peak (Figure 2D) suggesting that the water molecule is not displaced by the ligand and there is not a direct coordination of the nitrogen-containing imidazole ring to the heme iron. However, upon addition of histidine, a decrease at 418 nm that is not accompanied by an increase in the region 425-433 nm is observed in the difference spectra (inset Figure 2D). This behaviour has been previously reported for azole-containing ligands that can interact with the water molecule coordinated by the heme iron without its displacement [48,49].

The lack of water displacement by the histidine ligand is due to the formation of a hydrogen bonding network that trap the ligand in the active site (Figure 2C). Such a network includes hydrogen bonds with the side chain of Ser267 and water-mediated hydrogen bonds with the carbonyl group of Val262 and the side chain of Glu266.

The presence of a histidine molecule is particularly interesting since it has been recently shown that dual functional small molecules (DFSMs) containing histidine significantly increase the peroxygenase activity of mutants of cytochrome P450 BM3 [50,51].

As in most cytochromes P450, also in CYP116B5hd structure a water molecule that disrupts the H-bond pattern of helix I is present forming the kink region that has been proposed to accommodate the dioxygen during catalysis (Figure 2C) [52].

3.3 Substrate access channel and MD simulations

Analysis of the cavities of CYP116B5hd was performed using the CASTp 3.0 server [41]. This shows the presence of a catalytic pocket of 284 $Å^3$ in volume that is not connected to the protein surface (Figure 3A). The relatively small catalytic pocket of the protein is lined by residues that are well conserved across P450116B members and can be divided in 4 tiers, as suggested for CYP116B46hd [29] with the first three carrying the mostly hydrophobic amino acids and the forth tier formed by polar residues (Figure 3B). In CYP116B5 there are substitutions compared to CYP116B46 that can be found in most CYP116B members. In tier 1, Ser309 replaces the Pro residue of CYP116B46, Trp195 replaces a Phe in tier 3 and a Thr194 replaces an Ala in tier 4. Thus, there are non-conservative hydrophobic to hydrophilic substitutions that could reflect a different substrate profile and/or regioselectivity.

A 826 $Å^3$ cavity extending from the active site to the protein surface through a tunnel of about 14 Å in length was detected in CYP116B46hd (Figure 3C) [29]. The absence of such a tunnel in the CYP116B5hd structure suggests a closed conformation of the enzyme induced by the presence of a ligand. Indeed, cytochromes P450 are known to undergo conformational changes throughout their catalytic cycle and to switch from open to closed conformations to accommodate ligands in their active site [53-56]. In order to investigate possible movements in CYP116B5hd, molecular dynamics simulations were performed in the absence of any ligand. At the end of the simulation, movements of the C-D, E-F, F-G and G-H loops was found to trigger significant shifts

of B'-, G- and H-helices resulting in the opening of a tunnel from the catalytic pocket and the protein surface. The tunnel corresponds to the one detected in the crystal structure of CYP116B46 and to the 2a channel in the nomenclature proposed for cytochromes P450 (Figure 3D) [57].

During the simulation, the root mean square deviation (RMSD) converged after 60 ns (Figure 4A). The root mean square fluctuation (RMSF) profile as a function of residue shows that the most flexible regions of the protein are the C-D, E-F, F-G and G-H loops (Figure 4B, 4C). Moreover, the conformational change does not overcome a large energy barrier transition, as shown by the stability of the potential energy and secondary structure plots (Figure S2) indicating that the two states are energetically equivalent.

In order to support the results from the MD simulations, a time course of trypsin digestion was used to identify the most flexible loops in the protein on the basis that trypsin usually acts on basic residues exposed to the surface [58].

The time course of the trypsin digestion shown in Figure 4D indicates two main bands at around 38 kDa and 24 kDa. According to the prediction based on the amino acidic sequence, three cleavage sites are compatible with the generation of a fragment at around 38 kDa (Table S1). These sites are Lys83, Lys99 and Arg104, with the first one located on the loop connecting β2-3 and B'-helix, and the other two located on the B'-C loop. On the other hand, the only two trypsin-accessible sites that can give the bands at around 24 kDa are R197 and K231 that lie on the F-G and G-H loop, respectively.

These results are in line with MD simulations data and suggest that these loop regions are the most accessible and allow to open and close the channel identified by the CASTp server analysis.

3.4 Surface analysis and docking with the redox partner

The CYP116B5hd is physiologically part of a self-sufficient enzyme that possesses two reductase domains containing a FMN cofactor and a 2Fe-2S cluster [28].

As the heme proximal face in cytochromes P450 is known to be involved in electron transport chain from the electron donors, a comparison of the charge distribution in this area was carried out considering representative members of bacterial enzymes that need a reduction partner for catalysis (CYP102A1 or P450 BM3 and CYP101A1 or P450cam) and representative members of bacterial P450 peroxygenases (CYP152). As shown in Figure 5A, the two CYP116 enzymes have a positively charged patch in the centre of the proximal face forming a cavity pointing toward the heme prosthetic group. On the other hand, the presence of Asp and Glu residues in the loop connecting helices K' and L (arrow in figure 5A), introduces a negatively charged area that is also present in cytochromes P450 able to use the peroxide shunt (CYP152).

The interaction of cytochromes P450 with their redox partner is a very interesting aspect that controls P450 catalysis, as demonstrated for P450cam [59,60]. Nevertheless, little is known about the interaction between the different domains in class VII cytochromes P450. For this reason, a homology model was generated for the phthalate family oxygenase (PFOR)-like reductase domain containing FMN and 2Fe-2S clusters. The crystal structure of phthalate dioxygenase reductase from *Burkholderia cepacia* sharing 55% of sequence identity [61] was used as a template for homology modelling.

Structural data on the complexes P450ca-putidaredoxin (Pdx) and CYP11A1-adrenoxin (Adx) and CYP199A2-ferrodoxin (Pux) are available [62-65]. Thus, we docked the model of only the 2Fe-2S domain to CYP116B5hd crystal structure. The

best pose showed that the interaction occurs mainly through electrostatic interactions (Figure 5B).

When the electrostatic surface of Pdx, Adx, Pux and the CYP116B5 2Fe-2S domain are compared, the 2Fe-2S cluster protrudes from a negatively charged face in all cases (Figure 5C). On the other hand, when the electrostatic surfaces of the P450 enzymes are compared, while P450cam (PDB ID 4JWS), CYP11A1 (PDB ID 3N9Y) and CYP199A2 (PDB ID 2FR7) have an extended positively charged cluster in the proximal face, CYP116B6 has only a small cavity positively charged, that is formed by K66, R70, R119, K377 and R381 (Figure 5C).

In the Pdx-P450cam complex, the main interactions are the ionic pair Asp38-Arg112 and the H-bonds between Trp106 and Arg109-Asn116. In the CYP11A1-Adx complex, two salt bridges (Asp72-Lys339 and Asp76-Lys343) involve basic residues on the P450 proxymal side [64]. Also in the case of CYP199A2, three basic residues on the proximal face of the P450 enzyme are predicted to form salt bridges with acidic amino acids on Pux [65]. In CYP116B5 complex, three ion pairs are predicted to form. In particular, one basic (K377) and two acidic (E363 and D359) residues on the P450 proximal face are predicted to form three salt bridges with D283, R282 and R243 on the 2Fe-2S domain, respectively.

Another significant difference between the different complexes analysed, is the lack of the α3 helix in the 2Fe-2S domain of CYP116B5. Such a helix is important for the interaction with the C-helix of the P450 protein in class I cytochromes P450 [65].

3.5 Identification of structural determinants for peroxygenase activity

The isolated heme domain of CYP116B5 is able to use the peroxide shunt to drive its catalysis [27]. Its reduction potential is unusually high (-144 ± 42 mV) when compared

to other cytochromes P450 [27]. This is in keeping with the values found for other P450 peroxygenases [66]. Since it is known that the protein matrix is crucial to determine the reduction potential of the heme iron [67-69] and that the sensitivity of amino acids involved in electron transfer to hydrogen peroxide damage is important to drive catalysis through the peroxide shunt [70], a comparative analysis was performed on: a) the active site residues; b) the amino acids present in the loop containing the cysteine heme ligand; c) the amino acids involved in electron transfer. To this end, a structural alignment was performed with three members of the CYP152 family as representative members of P450 peroxygenases (CYP152A1, CYP152B1 and CYP152L1) and P450BM3 and P450cam as P450 enzymes that use the full canonical cycle. The findings from the analysis of the three points are:

a) For what concerns the active site residues, the conservation was found to be poor when considering CYP116B5 and peroxygenases (only 4 out of 18 residues are conserved), but higher when considering P450 BM3 and P450cam (7 and 9 out of 18, respectively) (Table 2). In particular, a highly conserved arginine residue that is known to form a bidentate interaction with the carboxylate moiety of fatty acid substrates is present in all the P450 peroxygenase. The arginine is usually followed by a proline residue and the Arg-Pro couple replaces the Asp-Thr motif present in all the other P450s. The acid-alcohol pair is considered crucial for protonation of heme iron-oxo species in the canonical P450 catalytic cycle [71,72]. However, in P450 peroxygenases there is no need of oxygen reduction and protonation steps. Interestingly, in CYP116B enzymes the acid-alcohol pair motif is present (Glu266-Thr267 in CYP116B5) whereas the Arg-Pro motif is absent. This suggests that the Arg-Pro motif is not crucial in driving the canonical catalytic cycle versus the peroxide shunt.

b) When considering the loop carrying the cysteine heme iron ligand, this is longer in P450 peroxygenases when compared to the one present in CYP116 members as well as P450 BM3 and P450cam (Figure 6). In P450 peroxygenases, there is an insertion of four residues that are not conserved among different CYP152 members. Moreover, it has been suggested that the strongly conserved Phe residue located seven amino acids upstream the Cys heme ligand in P450cam and BMP (in position 393 and 350 respectively) can be crucial for the modulation of the heme Fe(III)/Fe(II) reduction potential [73]. Indeed, in CYP152 members [66] and in BM3 F393A/H mutants [74] the potential is unusually high. However, the high reduction potential measured in CYP116B5hd seems not to be related to this Phe residue that is present in position 375 and conserved among CYP116B members. Nevertheless, significant substitutions are present in the loop carrying the cysteine ligand: 1) before the Cys heme ligand a hydrophobic residue is present in P450 BM3 (Ala) and P450cam (Leu) and it is replaced by a polar residue in CYP116B (Gln) and a charged residue (Arg) in CYP152 (Figure 6); 2) three amino acids before the heme ligand, a small aliphatic residue is present in peroxygenase and CYP116B that is replaced by a polar amino acid in P450 BM3 (Ser) and P450cam (Gln); 3) three residues after the Cys heme ligand at the beginning of helix L where we find a basic residue in CYP116B members, an acidic residue in P450 peroxygenases and a Gln residue in P450BM3 and P450cam.

c) The most sensitive residues to hydrogen peroxide damage within the ones involved in the electron transfer are Trp96 and Phe405 in P450 BM3 [70]. Indeed, the mutations Trp96Ala and Phe405Leu generated variants that resulted more stable in the presence of hydrogen peroxide. Table 3 shows that Trp96 is substituted by

Met115 in CYP116B5 and by a well conserved His (92 in CYP152L1) in P450 peroxygenases. Phe405 is replaced by an isoleucine in both enzymes.

In order to identify other hotspot positions that can favour the peroxide shunt, a mutant of P450 BM3 engineered by directed evolution to use the peroxide shunt was also taken into account [75]. The mutant called 21B3 and carrying 10 mutations was identified to have a 20-fold increased activity in presence of H_2O_2 and p-nitrophenylcarboxyacid (12-pNCA) as a substrate.

A structural alignment of CYP116B5hd with P450 BM3, the 21B3 mutant and CYP152L1 was performed (Table 3). The structural alignment shows that some of the residues introduced in the mutant of BM3 are present in one or both the peroxygenase enzymes (CYP116B5 and CYP152L1). For many of these residues it is difficult to predict the effect of the amino acid substitution due to their location that is not within the active site nor in the the substrate binding channel or F-G helices. Nevertheless, His100 is four amino acids apart in the same helix as Trp96 that is known to be involved in electron transfer in P450 BM3 [70]. In CYP116B5 and CYP152L1, the presence of Arg and Lys in the same position as His100 is important to establish different interactions with the backbone carbonyl of the proximal loop containing the Cys heme ligand.

Taken together, these data show that specific substitutions in the proximal loop carrying the cysteine heme ligand and in amino acids involved in electron transfer are crucial to confer to CYP116B5hd a higher reduction potential and a higher tolerance to hydrogen peroxide.

3.6 Substrate docking

The availability of the crystal structure of CYP116B5 allows to predict how the interaction between the P450 enzyme and three substrates known to be oxidised by CYP116B5hd [27] occur using molecular docking simulations. The Autodock algorithm yielded several poses for each ligand that were scored according to their binding energy. The theoretical binding energy, binding constant (K_d) values and the residues predicted to interact with the substrates are reported in Table 4 with the highest binding energy (indicating a higher affinity to the target) predicted for tamoxifen.

Figure 7 shows the best poses obtained for the three compounds, together with the predicted interacting amino acids. For *p*-nitrophenol, the nitro moiety is predicted to form 3 H-bonds with the hydroxyl group of Thr105 and the backbone groups of Leu106 and Val107, respectively. The hydroxyl-substituted carbon atom of the phenol aromatic ring is the closest to the heme iron, consistent with the formation of *p*-nitrocatechol (Figure 7). For the drugs diclofenac and tamoxifen, the protein-substrate binding occurs mainly through hydrophobic interactions (Table 4, Figure 7). However, three aromatic residues (Trp195, Trp313 and Phe413), located in the substrate access channel, seem to play a crucial role in substrate gating and thus can be the target for future mutagenesis.

In the case of diclofenac, the best pose is compatible with the hydroxylation of the non-substituted aromatic ring at C5. The dimethylethanamine moiety of tamoxifen is found to face the heme iron in a pose compatible with the previuosly observed N-demethylation reaction that the enzyme is able to catalyse on this substrate [27].

4. Conclusions

In conclusion, the crystal structure of CYP116B5hd is the first example of a class VII cytochrome P450 in a closed conformation and provides the basis for the design of new biocatalysts with the desired selectivity. Moreover, this protein shares some features with bacterial enzymes that require a reduction partner as well as with P450 peroxygenases. A detailed structural alignment allowed the identification of residues responsible for the peroxygenase activity with the proximal loop carrying the cys-ligand and the negative patches present around the heme proximal site playing a crucial role. It can be foreseen that these residues can be the target for site directed mutagenesis studies directed to improve the stability and the activity of the enzyme in the presence of hydrogen peroxide.

Accession numbers

Coordinates and structure factor amplitudes have been deposited in the Protein Data Bank with accession number 6RO8.

References

1. H.P. Meyer, E. Eichhorn, S. Hanlon, S. Lütz, M. Schürmann, R. Wohlgemuth, R. Coppolecchia, The use of enzymes in organic synthesis and the life sciences: perspectives from the Swiss Industrial Biocatalysis Consortium (SIBC), Catal. Sci. Technol. 3 (2013) 29–40. doi:10.1039/C2CY20350B.

2. T. Hudlicky, J.W. Reed, Applications of biotransformations and biocatalysis to complexity generation in organic synthesis, Chem. Soc. Rev. 38 (2009) 3117. doi:10.1039/b901172m.

3. E.M. Isin, F.P. Guengerich, Kinetics and Thermodynamics of Ligand Binding by Cytochrome P450 3A4, J. Biol. Chem. 281 (2006) 9127–9136. doi:10.1074/jbc.M511375200.

4. F.P. Guengerich, A.W. Munro, Unusual Cytochrome P450 Enzymes and Reactions, J. Biol. Chem. 288 (2013) 17065–17073. doi:10.1074/jbc.R113.462275.

5. X. Zhang, S. Li, Expansion of chemical space for natural products by uncommon P450 reactions, Nat. Prod. Rep. 34 (2017) 1061–1089. doi:10.1039/C7NP00028F.

6. R. Bernhardt, V.B. Urlacher, Cytochromes P450 as promising catalysts for biotechnological application: chances and limitations, Appl. Microbiol. Biotechnol. 98 (2014) 6185–6203. doi:10.1007/s00253-014-5767-7.

7. Y. Wei, E.L. Ang, H. Zhao, Recent developments in the application of P450 based biocatalysts, Curr. Opin. Chem. Biol. 43 (2018) 1–7. doi:10.1016/j.cbpa.2017.08.006.

8. G. Di Nardo, G. Gilardi, Optimization of the bacterial cytochrome P450 BM3 system for the production of human drug metabolites, Int. J. Mol. Sci. 13 (2012) 15901–15924. doi:10.3390/ijms131215901.

9. S.C. Hammer, G. Kubik, E. Watkins, S. Huang, H. Minges, F.H. Arnold, Anti-Markovnikov alkene oxidation by metal-oxo–mediated enzyme catalysis, Science. 358 (2017) 215–218. doi:10.1126/science.aao1482.

10. O.F. Brandenberg, R. Fasan, F.H. Arnold, Exploiting and engineering hemoproteins for abiological carbene and nitrene transfer reactions, Curr. Opin. Biotechnol. 7 (2017) 102–111. doi:10.1016/j.copbio.2017.06.005.

11. L.H. Xu, Y.L. Du, Rational and semi-rational engineering of cytochrome P450s for biotechnological applications, Synth. Syst. Biotechnol. 3 (2018) 283–290. doi:10.1016/j.synbio.2018.10.001.

12. V.B. Urlacher, M. Girhard, Cytochrome P450 Monooxygenases in biotechnology and synthetic biology, Trends Biotechol. 37 (2019) 882–897. doi:10.1016/j.tibtech.2019.01.001.

13. R.K. Zhang, X. Huang, F.H. Arnold, Selective C H bond functionalization with engineered heme proteins: new tools to generate complexity, Curr. Opin. Chem. Biol. 49 (2019) 67–75. doi:10.1016/j.cbpa.2018.10.004.

14. J. Sasaki, A. Mikami, K. Mizoue, S. Omura, Transformation of 25- and 1 alpha-hydroxyvitamin D3 to 1 alpha, 25-dihydroxyvitamin D3 by using Streptomyces sp. strains, Appl. Environ. Microbiol. 57 (1991) 2841–2846.

15. J. Sasaki, A. Miyazaki, M. Saito, T. Adachi, K. Mizoue, K. Hanada, S. Omura, Transformation of vitamin D3 to 1α,25-dihydroxyvitamin D3 via 25-hydroxyvitamin D3

using Amycolata sp. strains, Appl. Microbiol. Biotechnol. 38 (1992). doi:10.1007/BF00174460.

16. D.K. Ro, E.M. Paradise, M. Ouellet, K.J. Fisher, K.L. Newman, J.M. Ndungu, K.A. Ho, R.A. Eachus, T.S. Ham, J. Kirby, M.C.Y. Chang, S.T. Withers, Y. Shiba, R. Sarpong, J.D. Keasling, Production of the antimalarial drug precursor artemisinic acid in engineered yeast, Nature. 440 (2006) 940–943. doi:10.1038/nature04640.

17. C.J. Paddon, P.J. Westfall, D.J. Pitera, K. Benjamin, K. Fisher, D. McPhee, M.D. Leavell, A. Tai, A. Main, D. Eng, D.R. Polichuk, K.H. Teoh, D.W. Reed, T. Treynor, J. Lenihan, H. Jiang, M. Fleck, S. Bajad, G. Dang, D. Dengrove, D. Diola, G. Dorin, K.W. Ellens, S. Fickes, J. Galazzo, S.P. Gaucher, T. Geistlinger, R. Henry, M. Hepp, T. Horning, T. Iqbal, L. Kizer, B. Lieu, D. Melis, N. Moss, R. Regentin, S. Secrest, H. Tsuruta, R. Vazquez, L.F. Westblade, L. Xu, M. Yu, Y. Zhang, L. Zhao, J. Lievense, P.S. Covello, J.D. Keasling, K.K. Reiling, N.S. Renninger, J.D. Newman, High-level semi-synthetic production of the potent antimalarial artemisinin, Nature. 496 (2013) 528–532. doi:10.1038/nature12051.

18. K. Yasuda, H. Sugimoto, K. Hayashi, T. Takita, K. Yasukawa, M. Ohta, M. Kamakura, S. Ikushiro, Y. Shiro, T. Sakaki, Protein engineering of CYP105s for their industrial uses, Biochim. Biophys. Acta Proteins Proteom. 1866 (2018) 23–31. doi:10.1016/j.bbapap.2017.05.014.

19. F. Hannemann, A. Bichet, K.M. Ewen, R. Bernhardt, Cytochrome P450 systems—biological variations of electron transport chains, Biochim. Biophys. Acta – Gen. Subjects. 1770 (2007) 330–344. doi:10.1016/j.bbagen.2006.07.017.

20. E.G. Hrycay, J.A. Gustafsson, M. Ingelman-Sundberg, L. Ernster, Sodium periodate, sodium chlorite, and organic hydroperoxides as hydroxylating agents in

hepatic microsomal steroid hydroxylation reactions catalyzed by cytochrome P-450, FEBS Lett. 56 (1975) 161–165. doi:10.1016/0014-5793(75)80132-3.

21. G.A. Roberts, A. Çelik, D.J.B. Hunter, T.W.B. Ost, J.H. White, S.K. Chapman, N.J. Turner, S.L. Flitsch, A Self-sufficient cytochrome P450 with a primary structural organization that includes a flavin domain and a [2Fe-2S] redox center, J. Biol. Chem. 278 (2003) 48914–48920. doi:10.1074/jbc.M309630200.

22. R. De Mot, A.H.A. Parret, A novel class of self-sufficient cytochrome P450 monooxygenases in prokaryotes, Trends Microbiol. 10 (2002) 502–508. doi:10.1016/S0966-842X(02)02458-7.

23. L. Liu, R.D. Schmid, V.B. Urlacher, Engineering cytochrome P450 monooxygenase CYP 116B3 for high dealkylation activity, Biotechnol. Lett. 32 (2010) 841–845. doi:10.1007/s10529-010-0233-9.

24. Y.C. Yin, H.L. Yu, Z.J. Luan, R.J. Li, P.F. Ouyang, J. Liu, J.H. Xu, Unusually broad substrate profile of self-sufficient cytochrome P450 monooxygenase CYP116B4 from Labrenzia aggregata, ChemBioChem. 15 (2014) 2443–2449. doi:10.1002/cbic.201402309.

25. J.L. Porter, S. Sabatini, J. Manning, M. Tavanti, J.L. Galman, N.J. Turner, S.L. Flitsch, Cloning, expression and characterisation of P450-Hal1 (CYP116B62) from Halomonas sp. NCIMB 172: A self-sufficient P450 with high expression and diverse substrate scope, Enzyme Microb. Technol. 113 (2018) 1–8. doi:10.1016/j.enzmictec.2018.02.005.

26. M. Tavanti, J.L. Porter, S. Sabatini, N.J. Turner, S.L. Flitsch, Panel of new thermostable CYP116B self-sufficient cytochrome P450 monooxygenases that

catalyze C−H activation with a diverse substrate scope, ChemCatChem. 10 (2018) 1042–1051. doi:10.1002/cctc.201701510.

27. A. Ciaramella, G. Catucci, G. Di Nardo, S. Sadeghi, G. Gilardi, Peroxide-driven catalysis of the heme domain of A. radioresistens cytochrome P450 116B5 for sustainable aromatic rings oxidation and drug metabolites production. New Biotech. (2019) – Accepted.

28. D. Minerdi, S.J. Sadeghi, G. Di Nardo, F. Rua, S. Castrignanò, P. Allegra, G. Gilardi, CYP116B5: a new class VII catalytically self-sufficient cytochrome P450 from A cinetobacter radioresistens that enables growth on alkanes: oxidation of n -alkanes by a novel self-suffcient bacterial cytochrome P450, Mol. Microbiol. 95 (2015) 539–554. doi:10.1111/mmi.12883.

29. M. Tavanti, J.L. Porter, C.W. Levy, J.R. Gómez Castellanos, S.L. Flitsch, N.J. Turner, The crystal structure of P450-TT heme-domain provides the first structural insights into the versatile class VII P450s, Biochem. Biophys. Res. Commun. 501 (2018) 846–850. doi:10.1016/j.bbrc.2018.05.014.

30. T. Omura, R. Sato, The carbon monoxide-binding pigment of liver microsomes. I. Evidence for its hemoprotein nature, J. Biol. Chem. 239 (1964) 2370–2378.

31. M.T.B. Clabbers, T. Gruene, J.M. Parkhurst, J.P. Abrahams, D.G. Waterman, Electron diffraction data processing with DIALS, Acta Crystallogr. D Biol. Crystallogr. 74 (2018) 506–518. doi:10.1107/S2059798318007726.

32. P.R. Evans, G.N. Murshudov, How good are my data and what is the resolution?, Acta Crystallogr. D Biol. Crystallogr. 69 (2013) 1204–1214. doi:10.1107/S0907444913000061.

33. B.W. Matthews, Solvent content of protein crystals. J. Mol. Biol. 33 (1968) 491–497.

34. A.J. McCoy, R.W. Grosse-Kunstleve, P.D. Adams, M.D. Winn, L.C. Storoni, R.J. Read, Phaser crystallographic software, J. Appl. Crystallogr. 40 (2007) 658–674. doi:10.1107/S0021889807021206.

35. M.D. Winn, C.C. Ballard, K.D. Cowtan, E.J. Dodson, P. Emsley, P.R. Evans, R.M. Keegan, E.B. Krissinel, A.G.W. Leslie, A. McCoy, S.J. McNicholas, G.N. Murshudov, N.S. Pannu, E.A. Potterton, H.R. Powell, R.J. Read, A. Vagin, K.S. Wilson, Overview of the CCP4 suite and current developments, Acta Crystallogr. D Biol. Crystallogr. 67 (2011) 235–242. doi:10.1107/S0907444910045749.

36. T.C. Terwilliger, R.W. Grosse-Kunstleve, P.V. Afonine, N.W. Moriarty, P.H. Zwart, L.W. Hung, R.J. Read, P.D. Adams, Iterative model building, structure refinement and density modification with the PHENIX AutoBuild wizard, Acta Crystallogr. D Biol. Crystallogr. 64 (2008) 61–69. doi:10.1107/S090744490705024X.

37. P. Emsley, K. Cowtan, Coot : model-building tools for molecular graphics, Acta Crystallogr. D Biol. Crystallogr. 60 (2004) 2126–2132. doi:10.1107/S0907444904019158

38. G.N. Murshudov, A.A. Vagin, E.J. Dodson, Refinement of macromolecular structures by the maximum-likelihood method, Acta Crystallogr. D Biol. Crystallogr. 53 (1997) 240–255. doi:10.1107/S0907444996012255.

39. P.V. Afonine, R.W. Grosse-Kunstleve, N. Echols, J.J. Headd, N.W. Moriarty, M. Mustyakimov, T.C. Terwilliger, A. Urzhumtsev, P.H. Zwart, P.D. Adams, Towards

automated crystallographic structure refinement with phenix.refine, Acta Crystallogr. D Biol. Crystallogr. 68 (2012) 352–367. doi:10.1107/S0907444912001308.

40. V.B. Chen, W.B. Arendall, J.J. Headd, D.A. Keedy, R.M. Immormino, G.J. Kapral, L.W. Murray, J.S. Richardson, D.C. Richardson, MolProbity : all-atom structure validation for macromolecular crystallography, Acta Crystallogr. D Biol. Crystallogr. 66 (2010) 12–21. doi:10.1107/S0907444909042073.

41. W. Tian, C. Chen, X. Lei, J. Zhao, J. Liang, CASTp 3.0: computed atlas of surface topography of proteins, Nucleic Acids Res. 46 (2018) W363–W367. doi:10.1093/nar/gky473.

42. E. Krieger, G. Koraimann, G. Vriend, Increasing the precision of comparative models with YASARA NOVA--a self-parameterizing force field, Proteins. 47 (2002) 393–402. doi: 10.1002/prot.10104.

43. D.S. Goodsell, A.J. Olson, Automated docking of substrates to proteins by simulated annealing, Proteins: Struct. Funct. Bioinf. 8 (1990) 195–202. doi:10.1002/prot.340080302.

44. C. Gao, G. Catucci, G. Di Nardo, G. Gilardi, S.J. Sadeghi, Human flavin-containing monooxygenase 3: Structural mapping of gene polymorphisms and insights into molecular basis of drug binding, Gene. 593 (2016) 91–99. doi:10.1016/j.gene.2016.08.020.

45. D. Kozakov, D.R. Hall, B. Xia, K.A. Porter, D. Padhorny, C. Yueh, D. Beglov, S. Vajda, The ClusPro web server for protein–protein docking, Nat. Protoc. 12 (2017) 255–278. doi:10.1038/nprot.2016.169.

46. G. Di Nardo, G. Cimicata, R. Baravalle, V. Dell'Angelo, A. Ciaramella, G. Catucci, P. Ugliengo, G. Gilardi, Working at the membrane interface: Ligand-induced changes in dynamic conformation and oligomeric structure in human aromatase, Biotechnol. Appl. Biochem. 65 (2018) 46–53. doi:10.1002/bab.1613

47. J.K. Yano, L.S. Koo, D.J. Schuller, H. Li, P.R. Ortiz de Montellano, T.L. Poulos, Crystal structure of a thermophilic cytochrome P450 from the archaeon Sulfolobus solfataricus, J. Biol. Chem. 275 (2000) 31086–31092. doi:10.1074/jbc.M004281200.

48. S. Maurelli, M. Chiesa, E. Giamello, G. Di Nardo, V.E.V. Ferrero, G. Gilardi, S. Van Doorslaer, Direct spectroscopic evidence for binding of anastrozole to the iron heme of human aromatase. Peering into the mechanism of aromatase inhibition. Chem. Comm. 47 (2011) 10737-10739. doi: 10.1039/c1cc13872c.

49. K.P. Conner, A.A. Cruce, M.D. Krzyaniak, A.M. Schimpf, D.J. Frank, P. Ortiz de Montellano, W.M. Atkins, M.K. Bowman, Drug modulation of water–heme interactions in low-spin P450 complexes of CYP2C9d and CYP125A1, Biochemistry. 54 (2015) 1198–1207. doi:10.1021/bi501402k.

50. S.J.P. Willot, F. Tieves, M. Girhard, V.B. Urlacher, F. Hollmann, G. De Gonzalo, P450BM3-catalyzed oxidations employing dual functional small molecules, Catalysts. 9 (2019) 567. doi:10.3390/catal9070567.

51. J. Chen, F. Kong, N. Ma, P. Zhao, C. Liu, X. Wang, Z. Cong, Peroxide-driven hydroxylation of small alkanes catalyzed by an artificial P450BM3 peroxygenase system, ACS Catal. 9 (2019) 7350–7355. doi:10.1021/acscatal.9b02507.

52. T.L. Poulos, B.C. Finzel, A.J. Howard, High-resolution crystal structure of cytochrome P450cam, J. Mol. Biol. 195 (1987) 687–700. doi:10.1016/0022-2836(87)90190-2.

53. H. Li, T.L. Poulos, The structure of the cytochrome p450BM-3 haem domain complexed with the fatty acid substrate, palmitoleic acid, Nat. Struct. Biol. 4 (1997) 140–146.

54. D. Basudhar, Y. Madrona, S. Kandel, J.N. Lampe, C.R. Nishida, P.R.O. de Montellano, Analysis of cytochrome P450 CYP119 ligand-dependent conformational dynamics by two-dimensional NMR and x-ray crystallography, J. Biol. Chem. 290 (2015) 10000–10017. doi:10.1074/jbc.M114.627935.

55. A.M. Colthart, D.R. Tietz, Y. Ni, J.L. Friedman, M. Dang, T.C. Pochapsky, Detection of substrate-dependent conformational changes in the P450 fold by nuclear magnetic resonance, Sci. Rep. 6 (2016). doi:10.1038/srep22035.

56. I.K. Jóźwik, F.M. Kiss, Ł. Gricman, A. Abdulmughni, E. Brill, J. Zapp, J. Pleiss, R. Bernhardt, A.M.W.H. Thunnissen, Structural basis of steroid binding and oxidation by the cytochrome P450 CYP109E1 from Bacillus megaterium, FEBS J. 283 (2016) 4128–4148. doi:10.1111/febs.13911.

57. V. Cojocaru, K. Balali-Mood, M.S.P. Sansom, R.C. Wade, Structure and dynamics of the membrane-bound cytochrome P450 2C9, PLoS Comput. Biol. 7 (2011) e1002152. doi:10.1371/journal.pcbi.1002152.

58. A. Fontana, P.P. de Laureto, B. Spolaore, E. Frare, P. Picotti, M. Zambonin, Probing protein structure by limited proteolysis, Acta Biochim. Pol. 51 (2004) 299–321. doi:035001299.

59. S.H. Liou, M. Mahomed, Y.T. Lee, D.B. Goodin, Effector roles of putidaredoxin on cytochrome P450cam conformational states, J. Am. Chem. Soc. 138 (2016) 10163–10172. doi:10.1021/jacs.6b04110.

60. D. Batabyal, L.S. Richards, T.L. Poulos, Effect of redox partner binding on cytochrome P450 conformational dynamics, J. Am. Chem. Soc. 139 (2017) 13193–13199. doi:10.1021/jacs.7b07656.

61. C. Correll, C. Batie, D. Ballou, M. Ludwig, Phthalate dioxygenase reductase: a modular structure for electron transfer from pyridine nucleotides to [2Fe-2S], Science. 258 (1992) 1604–1610. doi:10.1126/science.1280857.

62. S. Tripathi, H. Li, T.L. Poulos, Structural Basis for Effector Control and Redox Partner Recognition in Cytochrome P450, Science. 340 (2013) 1227–1230. doi:10.1126/science.1235797.

63. Y. Hiruma, M.A.S. Hass, Y. Kikui, W.-M. Liu, B. Ölmez, S.P. Skinner, A. Blok, A. Kloosterman, H. Koteishi, F. Löhr, H. Schwalbe, M. Nojiri, M. Ubbink, The structure of the cytochrome P450cam–putidaredoxin complex determined by paramagnetic nmr spectroscopy and crystallography, J. Mol. Biol. 425 (2013) 4353–4365. doi:10.1016/j.jmb.2013.07.006.

64. N. Strushkevich, F. MacKenzie, T. Cherkesova, I. Grabovec, S. Usanov, H.W. Park, Structural basis for pregnenolone biosynthesis by the mitochondrial monooxygenase system, Proc. Natl. Acad. Sci. USA. 108 (2011) 10139–10143. doi: 10.1073/pnas.1019441108.

65. A.M. Bowen, E.O.D. Johnson, F. Mercuri, N.J. Hoskins, R. Qiao, J.S.O. McCullagh, J.E. Lovett, S.G. Bell, W. Zhou, C.R. Timmel, L.L. Wong, J.R. Harmer, A

structural model of a P450-ferredoxin complex from orientation-selective double electron–electron resonance spectroscopy, J. Am. Chem. Soc. 140 (2018) 2514–2527. doi:10.1021/jacs.7b11056.

66. J. Belcher, K.J. McLean, S. Matthews, L.S. Woodward, K. Fisher, S.E.J. Rigby, D.R. Nelson, D. Potts, M.T. Baynham, D.A. Parker, D. Leys, A.W. Munro, Structure and biochemical properties of the alkene producing cytochrome P450 OleT JE (CYP152L1) from the Jeotgalicoccus sp. 8456 bacterium, J. Biol. Chem. 289 (2014) 6535–6550. doi:10.1074/jbc.M113.527325.

67. R.J. Kassner, Theoretical model for the effects of local nonpolar heme environments on the redox potentials in cytochromes, J. Am. Chem. Soc. 95 (1973) 2674–2677. doi:10.1021/ja00789a044.

68. R.J. Kassner, Effects of Nonpolar Environments on the Redox Potentials of Heme Complexes, Proc. Natl. Acad. Sci. USA. 69 (1972) 2263–2267. doi:10.1073/pnas.69.8.2263.

69. A.K. Churg, A. Warshel, Control of the redox potential of cytochrome and microscopic dielectric effects in proteins, Biochemistry. 25 (1986) 1675–1681. doi:10.1021/bi00355a035.

70. A. Vidal-Limón, S. Águila, M. Ayala, C.V. Batista, R. Vazquez-Duhalt, Peroxidase activity stabilization of cytochrome P450BM3 by rational analysis of intramolecular electron transfer, J. Inorg. Biochem. 122 (2013) 18–26. doi:10.1016/j.jinorgbio.2013.01.009.

71. S. Nagano, T.L. Poulos, T.L, Crystallographic study on the dioxygen complex of wild-type and mutant cytochrome P450cam. Implications for the dioxygen activation mechanism. J. Biol. Chem. 280 (2005) 31659-31663. doi: 10.1074/jbc.M505261200.

72. I.G. Denisov, T.M. Makris, S.G. Sligar, I. Schlichting, I, Structure and chemistry of cytochrome P450. Chem Rev. 105 (2005) 2253-2277. doi: 10.1021/cr0307143.

73. A.W. Munro, K.J. McLean, J.L. Grant, T.M. Makris, Structure and function of the cytochrome P450 peroxygenase enzymes, Biochem. Soc. Trans. 46 (2018) 183–196. doi:10.1042/BST20170218.

74. T.W.B. Ost, A.W. Munro, C.G. Mowat, P.R. Taylor, A. Pesseguiero, A.J. Fulco, A.K. Cho, M.A. Cheesman, M.D. Walkinshaw, S.K. Chapman, Structural and spectroscopic analysis of the F393H mutant of flavocytochrome P450 BM3, Biochemistry. 40 (2001) 13430–13438. doi:10.1021/bi010717e.

75. P.C. Cirino, F.H. Arnold, A self-sufficient peroxide-driven hydroxylation biocatalyst, Angew. Chem. 42 (2003) 3299–3301. doi:10.1002/anie.200351434.

76. C.A. Hasemann, R.G. Kurumbail, S.S. Boddupalli, J.A. Peterson, J. Deisenhofer, Structure and function of cytochromes P450: a comparative analysis of three crystal structures, Structure. 3 (1995) 41–62. doi:10.1016/S0969-2126(01)00134-4.

77. E. Gasteiger, C. Hoogland, A. Gattiker, S. Duvaud, M.R. Wilkins, R.D. Appel, A. Bairoch, Protein Identification and Analysis Tools on the ExPASy Server, in: J.M Walker (Ed.), The Proteomics Protocols Handbook, Humana Press, 2005, pp. 571-607.
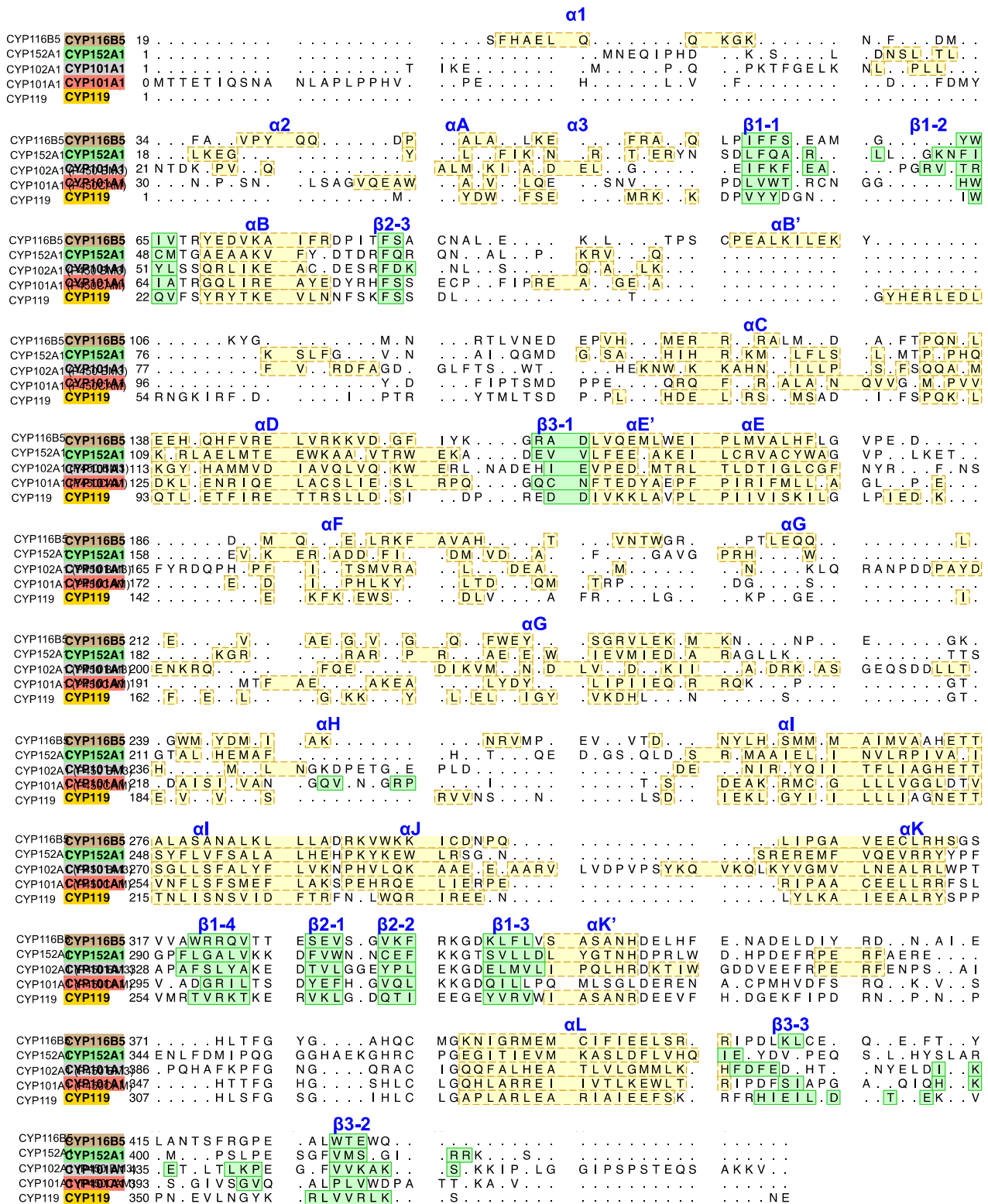
Appendix A. Supplementary data

Figure S1. Structural alignment between representative members of bacterial cytochromes P450 with the secondary structure elements of CYP116B5 labeled in blue. The yellow-boxed areas represent α-helices, the green-boxed areas show β-strands.
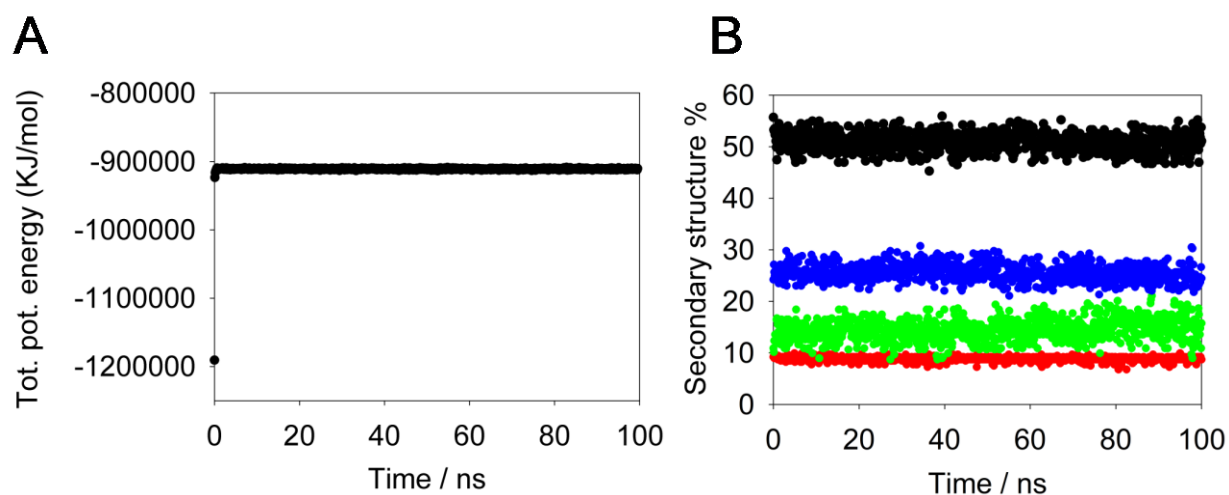
Figure S2. Plots of the A) potential energy and B) secondary structure changes during the 100 ns MD simulation carried out on CYP116B5hd crystal structure. The trace of α-helices is shown in black, β-sheets in red, turn in green and random coil in blue.

Table S1. Potential trypsin cleavage sites predicted by the server PeptideCutter [77].

Cleavage site	Digestion products		Location loop
K83	10.4	41.4	β2-3 – B'
K99	12.2	39.6	B' – C
R104	12.8	38.9	B' – C
K151	18.6	33.2	D –β3-1
R197	23.8	28	F – G
K231	27.7	24.1	G – H
R358	42	9.8	K' – h6
K399	46.8	5	β3-2 / β3-3
R414	48.6	3.2	β3-2 / β3-3

Tables

Table 1. Data collected and refinements statistics.

Data collection		
Space group	$P4_12_12$	
Cell dimensions	a=109.9 Å	α=90°
	b=109.9 Å	β=90°
	c=164.2 Å	γ=90°
Wavelength (Å)	1.0	
Resolution (Å)	2.6	
Average I/σ(I)	19.9 (1.50)	
Completeness (%)	100 (99.5)	
Redundancy	13.5 (12.1)	
$CC_{1/2}$	1.000 (0.584)	
Refinement		
Wilson B-factor (Å^2)	76.1	
Average B, all atoms (Å^2)	88.0	
R $_{work}$/R $_{free}$ (%)	0.20/0.24	
r.m.s.d. bond lengths (Å)	0.010	
r.m.s.d. bond angles (°)	1.112	
Overall quality		
Clashscore	11	
Ramachandran outliers	0.2%	
Sidechain outliers	2.5%	
RSRZ outliers	6.3%	

Table 2. Active site residues. Structural alignment of the two members of CYP116B subfamily with representative members of P450 peroxygenase (CYP152) and representative members of canonical P450s (P450 BM3 and P450 cam). The residue positions refer to CYP116B5 WT sequence.

Residue	CYP116B	CYP152	BMP	P450$_{cam}$
107	V	H/Q	F	T
263	A	P	A	G
267	T	I	T	T
309	S/P	P	T	L
310	V	F	A	V
313	W	L	F	D
80	V/A	M/A	L	P
105	T	I/V	S	I
259	A	D/E	T	L
413	F	/	T	V
81	L	L/M	/	/
195	F/W	F	/	T
262	V	N	I	V
266	E	R	E	D
190	H	M	A	L
191	T	I/A/R/D	M	T
193	N	S/A	/	M
194	A/T	F/A	/	T

Table 3. Residues potentially involved in hydrogen peroxide--driven catalysis. Structural alignment of CYP116B5hd with CYP152L1 (P450 peroxygenase), P450 BM3 WT and the mutant 21B3. The residue positions refer to P450 BM3 WT sequence.

Residue	CYP116B5	CYP152L1	BMP WT	BMP 21B3
58	V	A	I	V
100	R	K	H	R
107	F	L	F	L
135	K	F	A	S
145	L	S/I	M	V
239	D	H	N	H
274	A	D	S	T
434	Y	Y	K	E
446	T	I	V	I
87	V	H	F	A
96	M	H	W	A
405	I	I	F	L

Table 4. Substrate binding energy, predicted K$_d$ for CYP116B5hd structure calculated by AutoDock. The residues predicted to be involved in protein-substrate interaction are also listed.

Substrate	Binding energy (kcal/mol)	Dissociation constant (µM)	Contacting residues				
4-nitrophenol	4.59	14.67	LEU81 THR105 LEU106 VAL107	ALA189 HIS190			
Tamoxifen	11.15	0.67	ALA80 LEU81 GLU82 MET102	HIS190 THR194 TRP195	MET258 ALA259 VAL262 ALA263 ALA264 HIS265 GLU266 THR267	VAL310 ALA312 TRP313 ARG314	SER412 PHE413
Diclofenac	7.27	4.69	LEU81 THR105 VAL107	TRP195	MET256 ALA259 ILE260 VAL262 ALA263 GLU266 THR267 THR268	VAL310 TRP313	PHE413
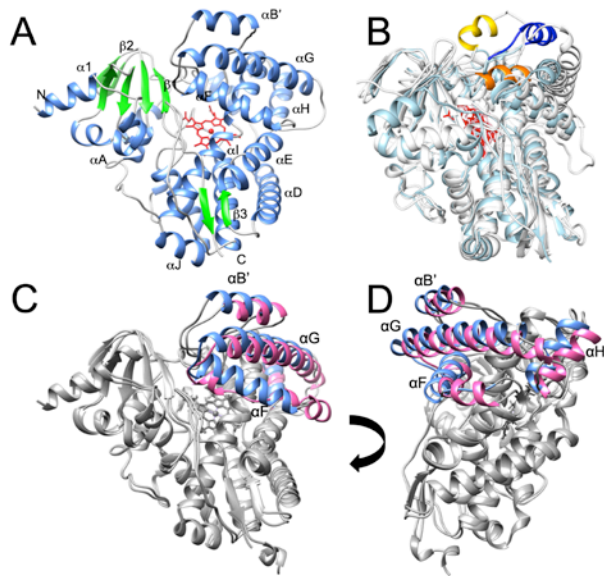
Figure

Figure 1. The crystal structure of CYP116B5hd. A) Overall structure coloured according to the secondary structure elements named according to the standard P450 nomenclature [76]. Superimposition of CYP116B5hd crystal structure with the B' helix in blue with the heme domain of P450 BM3 (PDB ID 2IJ2) and CYP119 (PDB ID 1IO7) where the same helix is in orange and yellow, respectively. C) Superimposition of the crystal structures of CYP116B5hd and CYP116B46hd. The structurally different regions are highlighted in blue and pink for CYP116B5hd and CYP116B46hd, respectively. The overall RMSD is 2.05 Å. D) Superimposition of the crystal structures of CYP116B5hd and CYP116B46hd rotated by 90°.
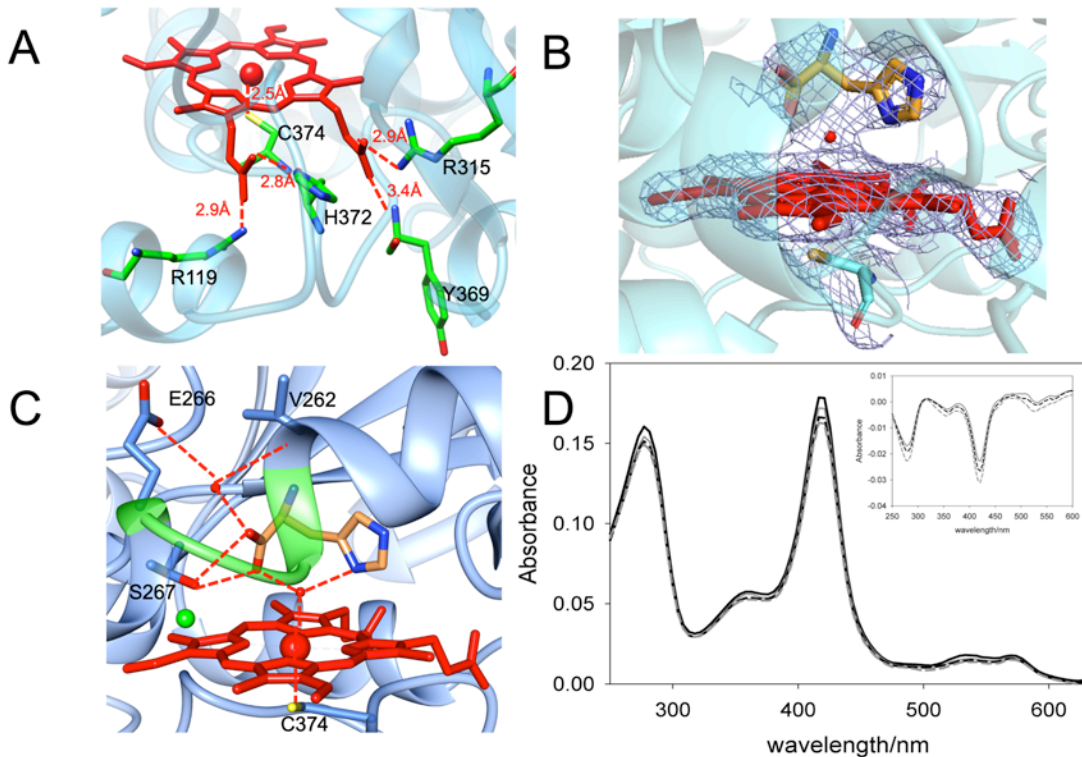
Figure 2. Active site of CYP116B5hd. A) Residues involved in heme binding in the active site of CYP116B5hd. B) Electron density of heme and the histidine ligand found in the active site of the protein. The 2Fobs-Fc map is contoured at a 1.0 σ level. C) Hydrogen bonding network involving Ser267, Val262, Glu266 and a water molecule stabilizing the histidine ligand in the active site of the enzyme. The kink region together with the water molecule that causes the disruption of helix I are shown in green. D) UV-vis spectra of ligand free CYP116B5hd (black line, 1.5 µM) and in complex with 25 µM (grey line), 100 µM (dashed black line) and 500 µM (dashed grey line) of histidine. Inset: Histidine-bound minus ligand free difference spectra showing a though at 418 nm and no corresponding increase at the wavelength typical of type I and II ligands.
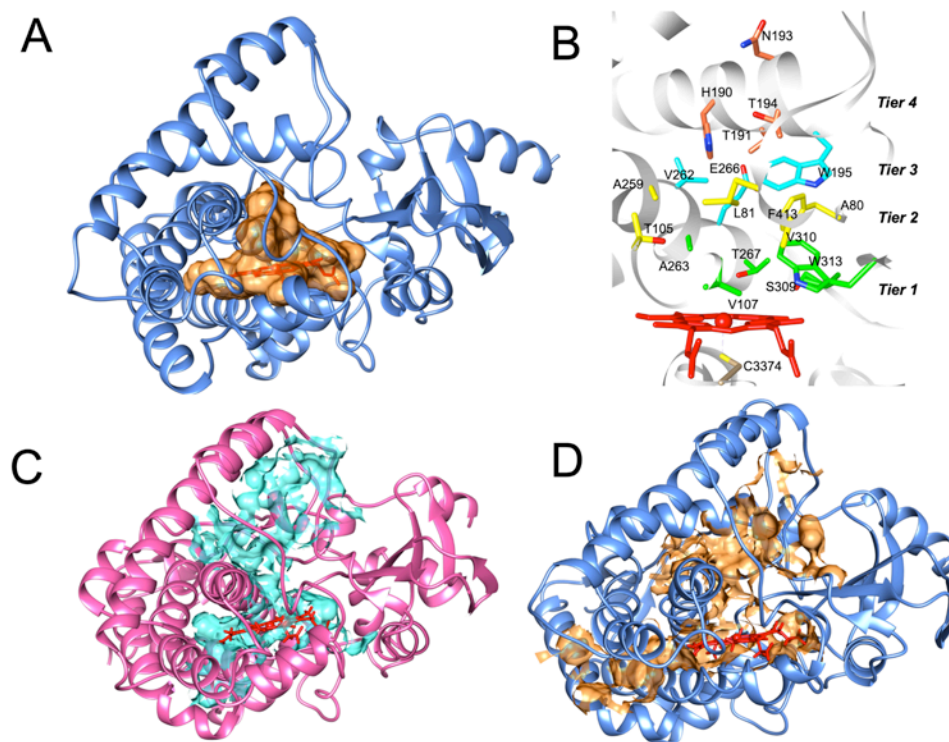
Figure 3. Analysis of protein cavities and substrate access channel. A) The main cavity predicted by the CASTp server on CYP116B5hd crystal structure. B) The residues forming the catalytic pocket of the enzyme are coloured according to 4 tiers. C) The main cavity predicted by the CASTp server of CYP116B46hd crystal structure and D) the main cavity predicted by the CASTp server for CYP116B5hd conformation after 100 ns simulation.
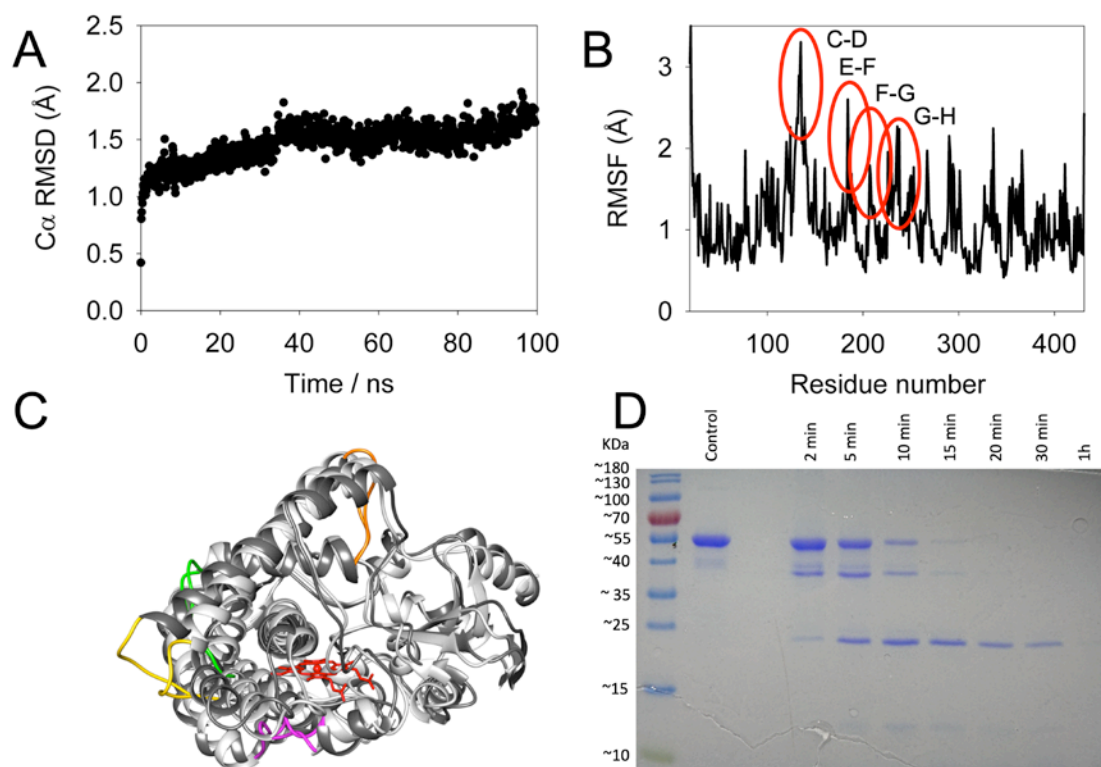

Figure 4. Results of MD simulations and their validation through trypsin digestion. A) Plot of the overall root mean square deviation (RMSD) of the Cα atoms of the protein as a function of the time of MD simulation. B) Plot of the root mean square fluctuations (RMSF) per residue obtained during the 100 ns simulation. C) Superimposition of the starting crystal structure of CYP116B5hd (light grey) with the last model obtained after 100 ns simulation (dark grey). The most flexible elements are colored in magenta (C-D loop), green (E-F loop), orange (F-G loop) and yellow (G-H loop). D) SDS-PAGE showing the time course of trypsin digestion.
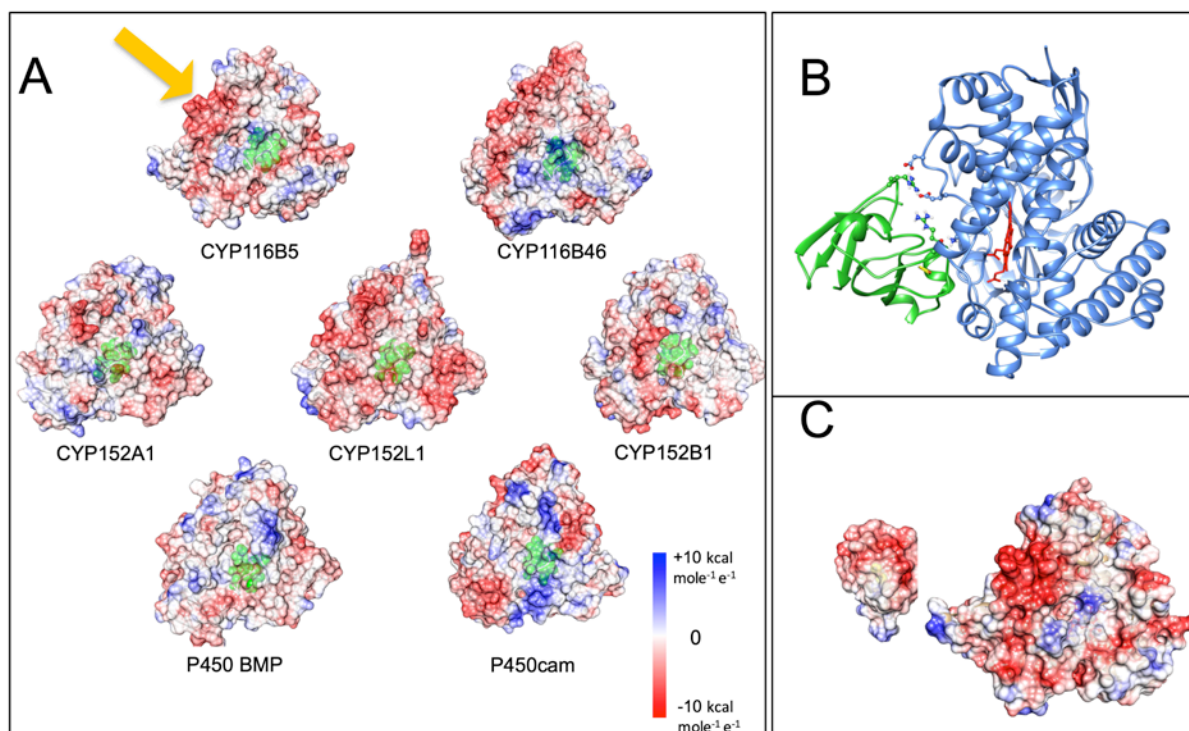
42

Figure 5. Surface electrostatics and docking with the redox partner. A) Surfaces electrostatics of CYP116B5hd compared to selected members of P450 peroxygenases (CYP152), P450 BM3 heme domain and P450cam. Surfaces are colored according to Coulomb's law calculation at a level of +10 (blue), 0 (white) and −10 (red) kcal mole^{-1} e^{-1}. The yellow arrow indicates the negative charges shared among CYP116B and P450 peroxygenase allocated in proximity of the a-helix K and L region. Heme is shown in green. B) Best docking cluster obtained by docking simulation using ClusPro server (weighted score of -579.5) of the 2Fe-2S cluster-containing domain with CYP116B5hd. The residues forming the main ion pairs at the proteins interface shown in sticks. C) Surface electrostatics of the interacting protein faces according to the docking simulations.
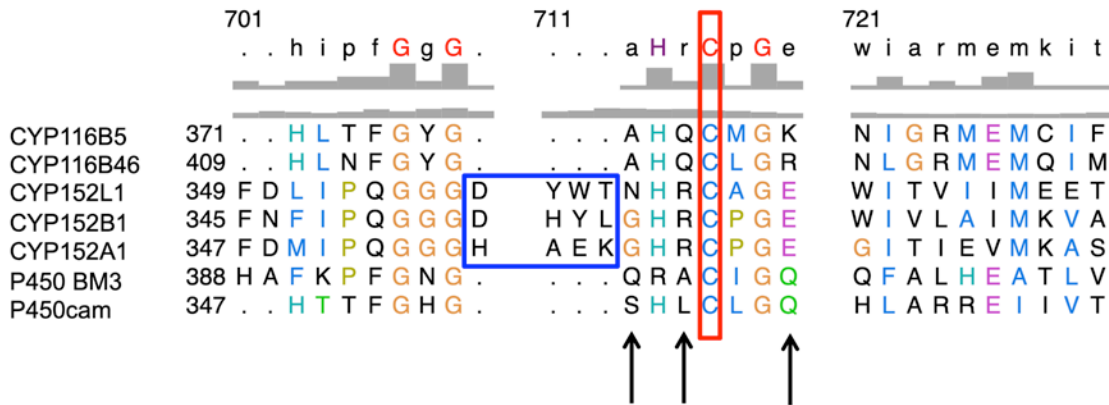
Figure 6. Structural alignment of bacterial P450s. Structural alignment between the two members of CYP116 family of known structure, representative members of P450 peroxygenases (CYP152) and representative members of cytochromes P450 that use the canonical P450 cycle for catalysis (P450 BM3 and P450cam). The cysteine heme ligand is boxed in red, the 4 amino acids insertion present in P450 peroxygenases in the loop carrying the Cys heme ligans ix boxed in blue. The arrows indicate non-conservative substitutions in the loop in positions that differ in CYP116B members, P450 peroxygenases and canonical P450 enzymes.
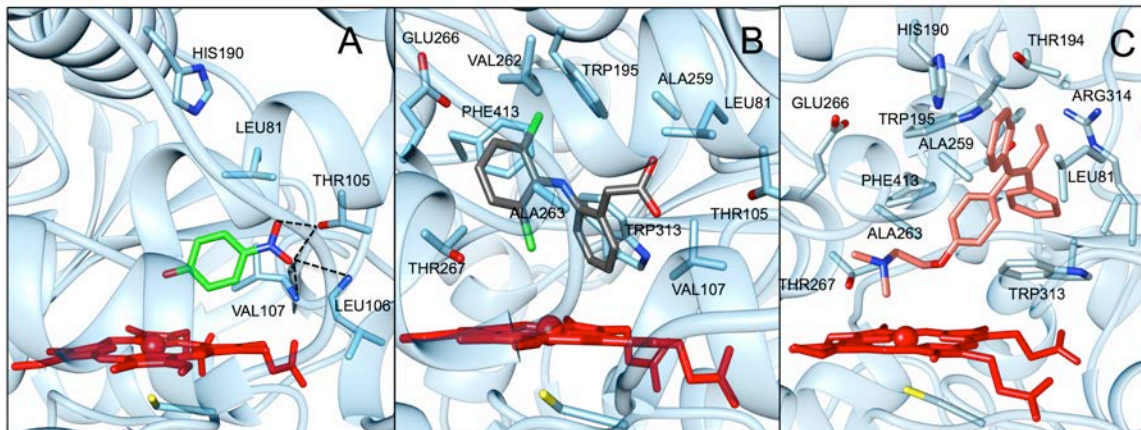

Figure 7. Best pose obtained from the docking simulation with known substrates of CYP116B5hd in hydrogen peroxide-dependent catalysis. The substrates are A) p-nitrophenol, B) diclofenac and C) tamoxifen.